Journal of Luminescence 132 (2012) 1345–1352

Contents lists available at SciVerse ScienceDirect

Journal of Luminescence

journal homepage: www.elsevier.com/locate/jlumin

Structural and photoluminescence investigation on the hot-wire assisted plasma enhanced chemical vapor deposition growth silicon nanowires

Su Kong Chong [a,*], Boon Tong Goh [a], Yuen-Yee Wong [c], Hong-Quan Nguyen [c], Hien Do [c], Ishaq Ahmad [d,e], Zarina Aspanut [a], Muhamad Rasat Muhamad [a], Chang Fu Dee [b], Saadah Abdul Rahman [a]

[a] Low Dimensional Materials Research Centre, Department of Physics, Faculty of Science, University of Malaya, 50603 Kuala Lumpur, Malaysia
[b] Institute of Microengineering and Nanoelectronics (IMEN), Universiti Kebangsaan Malaysia (UKM), Bangi, Selangor, Malaysia
[c] Department of Materials Science and Engineering, National Chiao Tung University, Hsinchu 30010, Taiwan
[d] Shanghai Institute of Applied Physics, Chinese Academy of Sciences, P.O. Box 800-204, 2019 Jialuo Road, Shanghai 201800, PR China
[e] Experimental Physics Labs, National Center for Physics, Quaid-i-Azam University, Islamabad 44000, Pakistan

ARTICLE INFO

Article history:
Received 22 May 2011
Received in revised form
3 January 2012
Accepted 19 January 2012
Available online 28 January 2012

Keywords:
Silicon nanowires
Hot-wire assisted plasma enhanced chemical vapor deposition
Structural
Photoluminescence

ABSTRACT

High density of silicon nanowires (SiNWs) were synthesized by a hot-wire assisted plasma enhanced chemical vapor deposition technique. The structural and optical properties of the as-grown SiNWs prepared at different rf power of 40 and 80 W were analyzed in this study. The SiNWs prepared at rf power of 40 W exhibited highly crystalline structure with a high crystal volume fraction, X_C of $\sim$82% and are surrounded by a thin layer of SiO_x. The NWs show high absorption in the high energy region ($E > 1.8$ eV) and strong photoluminescence at 1.73 to 2.05 eV (red–orange region) with a weak shoulder at 1.65 to 1.73 eV (near IR region). An increase in rf power to 80 W reduced the X_C to $\sim$65% and led to the formation of nanocrystalline Si structures with a crystallite size of <4 nm within the SiNWs. These NWs are covered by a mixture of uncatalyzed amorphous Si layer. The SiNWs prepared at 80 W exhibited a high optical absorption ability above 99% in the broadband range between 220 and $\sim$1500 nm and red emission between 1.65 and 1.95 eV. The interesting light absorption and photoluminescence properties from both SiNWs are discussed in the text.

© 2012 Elsevier B.V. All rights reserved.

1. Introduction

Considerable research efforts have been focused on one dimensional silicon nanowires (SiNWs) as devices and building blocks for future nanoelectronic applications due to their excellent structural [1–7], optical [8–13] and photoluminescence [14–29] properties. SiNWs possess different degrees of crystallinity, such as single crystalline [1–4], polycrystalline [31,32], nanocrystalline [33,34] and amorphous [35–38] structures depending on the techniques of synthesis and growth conditions. Highly crystalline SiNWs exhibit greater electron mobility than those with an amorphous structure [39]. Amorphous SiNWs on the other hand possess a better cycling performance in lithium batteries [40] and higher optical absorption [11] compared to crystalline NWs.

SiNWs exhibit a significant higher surface area to volume ratio than the bulk Si. Interaction of light with the subwavelength SiNWs could result in the total internal reflection, which causes a further reduction in the optical reflection and enhances the light trapping behavior of SiNWs. Excellent light absorption in SiNWs at the UV and visible region has been reported by several researchers [9–13]. Zhu et al. [11] investigated the light absorption ability of Si nanostructures for different angles of incidence at wavelength of 488 nm. They observed absorption above 90% at an angle of incidence up to 60° for Si nanocones. This effective photon absorption plus the high carrier collection abilities of SiNWs are believed to give great performance in photovoltaic applications. It could also lead to the development of the new generation of NW based solar cells.

SiNWs also exhibit room temperature visible light emission properties, which is absent in bulk material. The luminescence behavior in SiNWs is usually associated with quantum confinement effect [14–16], SiO_x (sub-oxide or silica) [17–20], suboxide defects at the SiO_x/Si interface [21–24], oxide related defect state [25,26], Si nanocrystallites within SiNWs [27] or any combination of these [28,29]. It is well-known that quantum confinement effect could only be considered if the diameter of NWs is less than 10 nm. For SiNWs with larger diameters, the surface species, such as Si nanocrystallites and oxide defect states are the main contributors to the luminescence properties. Besides, the luminescence characteristic of SiNWs is very much dependent on the morphology of the NWs. Sun et al. [27] reported that the chainlike SiNWs comprising of crystalline Si nanoparticles

* Corresponding author. Tel.: +603 79674147; fax: +603 79674146.
E-mail address: sukong1985@yahoo.com.my (S.K. Chong).

0022-2313/$ - see front matter © 2012 Elsevier B.V. All rights reserved.
doi:10.1016/j.jlumin.2012.01.026

interconnected by amorphous Si oxide NWs exhibit a much stronger emission intensity than the normal SiNWs. SiNWs are therefore potential materials for applications in light emitting diodes and nano-optoelectronic devices [30].

Chemical vapor deposition (CVD) combined with a catalyst induced vapor–liquid solid (VLS) process appears to be one of the most promising techniques to grow SiNWs due to its easy handling and controllable growth process. However, high temperature (~600 °C) is required to thermally decompose silane (SiH_4) gas into reactive radicals, which are responsible for the growth of SiNWs. In plasma enhanced chemical vapor deposition (PECVD), the dissociation of SiH_4 occurs at relatively low temperature. The growth of SiNWs at a much lower substrate temperature (< 400 °C) has been demonstrated by researchers [5–7,41]. In PECVD process, radio frequency (rf) power is an important parameter, which could affect the gas phase reactions in SiH_4 plasma and yield different combinations of Si_nH_m ionic radicals. By varying the rf power, the growth, crystallinity and optical properties of SiNWs can be controlled.

We have recently reported details on the synthesis of SiNWs on ITO coated glass substrates using hot-wire assisted PECVD technique [43]. High density of SiNWs was obtained using this technique. Direct preparation of SiNWs on this transparent substrate enables the optical measurements to be performed. In this work, we are reporting the results on a fundamental study done on the structural, optical and photoluminescence properties of these SiNWs.

2. Experimental methods

SiNWs were synthesized on ITO coated glass using a home-built hot-wire assisted PECVD system. Prior to the growth, the surface of the substrates were subjected to H_2 plasma for 5 min at substrate temperature and rf power of 400 °C and 40 W, respectively. The H_2 plasma leads to formation of In droplets on the surface of the substrates [42], which acted as catalyst for inducing growth of SiNWs. The sizes of the In droplets varying from 50 to 250 nm (average size $\sim 70 \pm 20$ nm). For SiNWs growth, SiH_4 and H_2 gases with flow rates of 5 and 150 sccm, respectively, were introduced into the reactor resulting in an increase in the pressure to 0.7 mbar within the reactor. The SiNWs samples were deposited for 30 min at rf powers of 40 W and 80 W. The details on the deposition procedures have been presented elsewhere [43].

The surface morphology of samples was examined by a FEI Quanta 200 field emission scanning electron microscope (FESEM). The structural properties and crystallinity of the SiNWs were studied by Raman spectroscopy, high resolution transmission electron microscopy (HRTEM) and selected area electron diffraction (SAED). Raman spectra of SiNWs were obtained from an InVia Reflex Raman microscope with a Raman imaging using Renishaw's StreamLine imaging method, at 532 nm diode laser excitation. The HRTEM images and SAED patterns were taken by a Philips Tecnai 20 TEM and a JEOL 2010 TEM. The attached electron-dispersive X-ray (EDX) spectroscope on JEOL 2010 TEM was employed to obtain the EDX spectra on SiNWs. The chemical composition of SiNWs was further investigated using a Jeol JAMP-9500 F Field Emission Auger Microprobe. With the high resolution of Auger electron imaging, the Auger electron spectra for single NWs can be obtained using a probe diameter of 8 nm. Fourier transform infrared (FTIR) spectra of samples were obtained from Perkin-Elmer System 2000 FTIR with a variable angle specular reflectance accessory attached on it. A JASCO V570 ultra-violet visible near-infrared (UV–vis-NIR) spectrophotometer was employed for optical transmission (T) and reflectance (R) measurements of samples at a range of 200–2200 nm with a Deuterium discharge tube (200–350 nm) and a Tungsten iodine lamp (330–2200 nm). Photoluminescence (PL) measurement was performed by the InVia Reflex PL microscope using Ar^+ laser with 514 nm of excitation wavelength.

3. Results and discussion

The morphologies of SiNWs synthesized at rf power of 40 and 80 W are represented by FESEM images as depicted in Fig. 1. The NWs are curve shaped and kinked, and are randomly grown overlapping each other. Most of the NWs show large catalyst droplets capped on top, which suggests that the typically vapor–liquid–solid (VLS) mechanism was taking place in the NWs growth. EDX and Auger measurements (not shown here) confirmed that capping droplets mainly consisted of In element. Due to the high wettability of In [41], the molten In droplets created a large contact angle (~125°) [44] and small contact area with the substrate. Thus, the NWs grown from the In droplets possessed much smaller diameter than the capping droplets. The diameters of SiNWs prepared at 40 W vary from 40 to 140 nm. Increase in rf power to 80 W results in the increase of the NWs density and broader NWs diameter distribution from 60 to 400 nm. The increase in NWs diameter distribution is due to the non-uniform side wall growth of the NWs mainly contributed by increase in SiH_n species reaching the nucleation sites at high rf power. Similar work reported by Adachi et al. [7], described

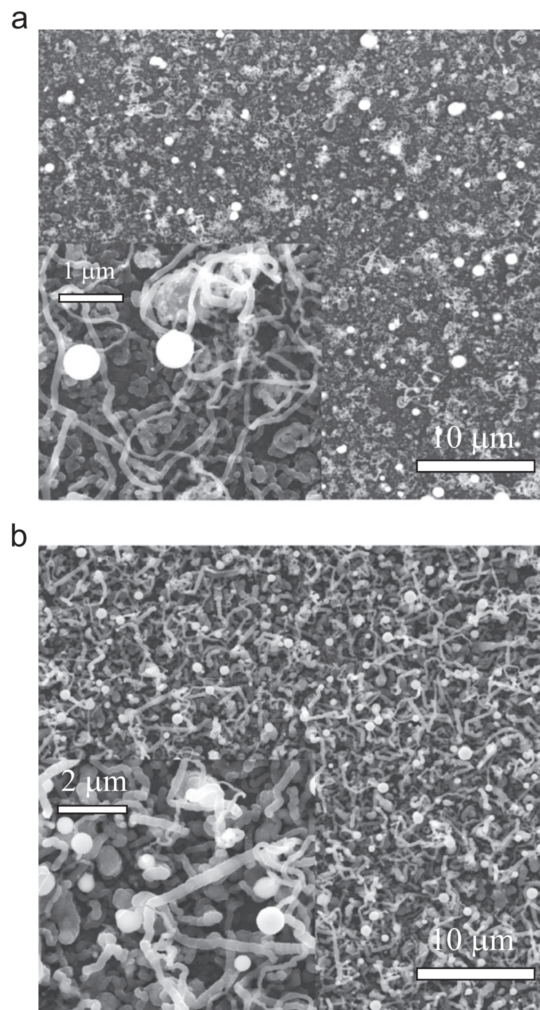

Fig. 1. FESEM images of SiNWs prepared by hot-wire assisted PECVD at rf power of (a) 40 W and (b) 80 W.

coverage of uncatalyzed amorphous Si layer on the walls of the SiNWs with increase in the rf power producing the plasma, resulting in an increase in diameter of the SiNWs.

Raman spectra with their corresponding Raman imaging features for SiNWs synthesized at rf power of 40 and 80 W are illustrated in Fig. 2. The brightness in Raman imaging features represents the crystalline structure of SiNWs. The Raman spectra taken from the SiNWs reveal a sharp peak located at $\sim$521 cm^{-1} together with a weak shoulder at a lower frequency of $\sim$480 cm^{-1}. The sharp peak corresponds to the TO phonon mode of crystal Si, while the weak shoulder is due to the amorphous structure in the SiNWs. The TO phonon modes of c-Si are shifted to a lower wavenumber of $\sim$517 and $\sim$512 cm^{-1} for SiNWs prepared at 40 and 80 W, respectively. Generally, the presence of nanocrystalline structures can contribute to the downshift due to the phonon confinement in SiNWs [45]. However, the irradiation of high laser power can also cause locally intense heating on the SiNWs and thus results in a further downshift in TO phonon mode [46–48]. In order to minimize this, we optimized the operating laser power before carried out the Raman measurements for the SiNWs. The shifting of Raman peaks is mainly attributed to the decrease in crystalline size and the formation of micro or nanocrystalline Si structure. The value of shifting in TO phonon mode is related to the crystallite size, D_R as [49]:

$$D_R = 2\pi\sqrt{\frac{B}{\Delta\omega}} \tag{1}$$

where B is 2.24 $cm^{-1}\,nm^2$ for Si and $\Delta\omega$ is the shifting of TO mode from c-Si peak located at 521 cm^{-1}. The D_R for SiNWs synthesized at 40 and 80 W are 4.2 ± 0.1 and 2.9 ± 0.1 nm, respectively. This indicates the existence of larger size Si nanocrystal formed on the surface or embedded in SiNWs prepared at 40 W compared to 80 W.

The Raman peaks of TO phonon modes are further deconvoluted by a Lorentzian function into three peaks corresponding to amorphous, grain boundary and crystalline components at 480 cm^{-1}, $\sim$500 cm^{-1} and 520 cm^{-1}, respectively, as depicted in Fig. 3. The crystalline volume fraction, X_C (in %) and grain boundary volume fraction, X_{GB} (in %) of the SiNWs can be calculated as [50,51]:

$$X_C = \frac{I_{520} + I_{500}}{\beta I_{480} + I_{520} + I_{500}} \times 100\% \tag{2}$$

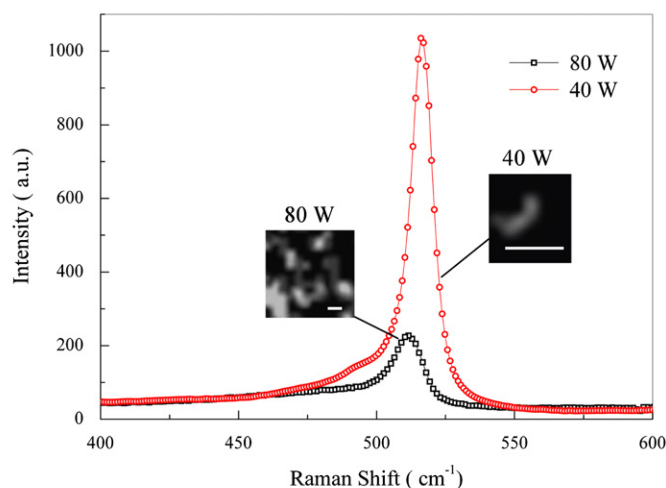

Fig. 2. Raman spectra of SiNWs synthesized at rf power of 40 and 80 W. The Raman imaging features of the SiNWs corresponded to the Raman spectra is inserted in figure (Scale bar = 1 μm).

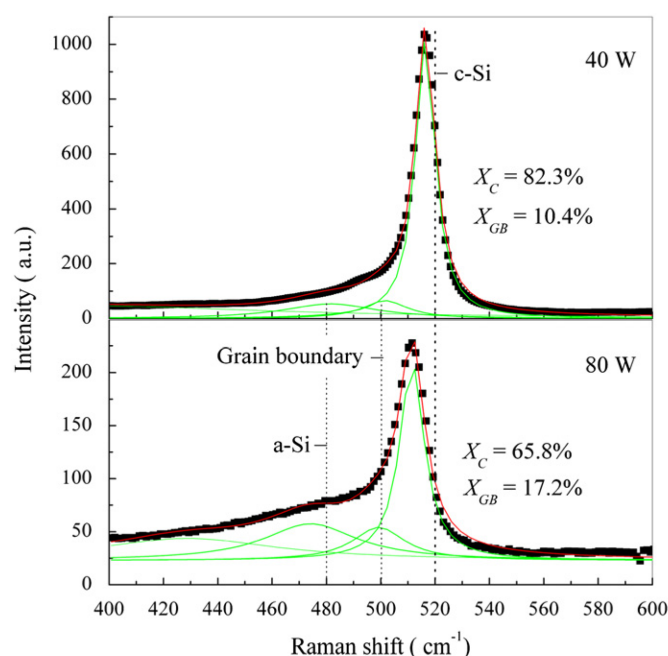

Fig. 3. Lorentzian fitted Raman spectra of SiNWs prepared at rf power of 40 and 80 W.

$$X_{GB} = \frac{I_{500}}{\beta I_{480} + I_{520} + I_{500}} \times 100\% \tag{3}$$

where I_{520}, I_{500} and I_{480} are integrated intensities of the crystalline, grain boundaries and amorphous components, respectively. The factor β is the ratio of the cross-section of the amorphous phase to the crystalline phase, which is defined as

$$\beta = 0.1 + \exp(-d/250) \tag{4}$$

where d is the grain size (in nm) [52]. The calculated X_C values reduce from 82.3 to 65.8%, however, X_{GB} is slightly increased from 10.4 to 17.2% for SiNWs synthesized at 40 and 80 W, respectively. The higher X_C in SiNWs prepared at 40 W indicates higher fractions of crystalline to amorphous structures, which might be due to the larger crystallite size as mentioned above. Similar to previous work [7], we observed that increase in rf power to 80 W reduces the X_C and increases the X_{GB} of the SiNWs. The lower X_C might correlate to the smaller crystallite size, while the higher X_{GB} suggests the formation of large amounts of Si nanocrystallites, which are surrounded by grain boundary components, embedded in the amorphous matrix of the SiNWs.

The crystallinity of the SiNWs prepared at different rf powers of 40 and 80 W were further examined by HRTEM. Fig. 4(a) shows the low magnification TEM image of SiNWs prepared at 40 W. The NWs exhibit a rough surface and are covered by a thin layer of SiO_x, with thickness of $\sim$2–3 nm. The HRTEM image of the SiNWs [enlarge from white framed region in Fig. 4(a)] illustrated in Fig. 4(b) reveals a long range of crystalline and a trace of amorphous structures. This indicates a highly crystalline structure of SiNWs prepared at a lower rf power of 40 W. Lattice dislocation due to twinning structures can be also observed within the NWs. The lattice spacing is about 0.31 nm, which corresponds to (111) crystalline orientation plane. The SAED pattern [Fig. 4(c)] reveals the discrete electron diffraction spots of crystal Si, which confirms the highly crystalline structure of the NWs. The TEM and HRTEM (enlarged from the TEM image) images of SiNWs prepared at rf power of 80 W are shown in Fig. 4(d) and (e), respectively. The SiO_x shell could not be clearly observed on the surface of the SiNW prepared at 80 W.

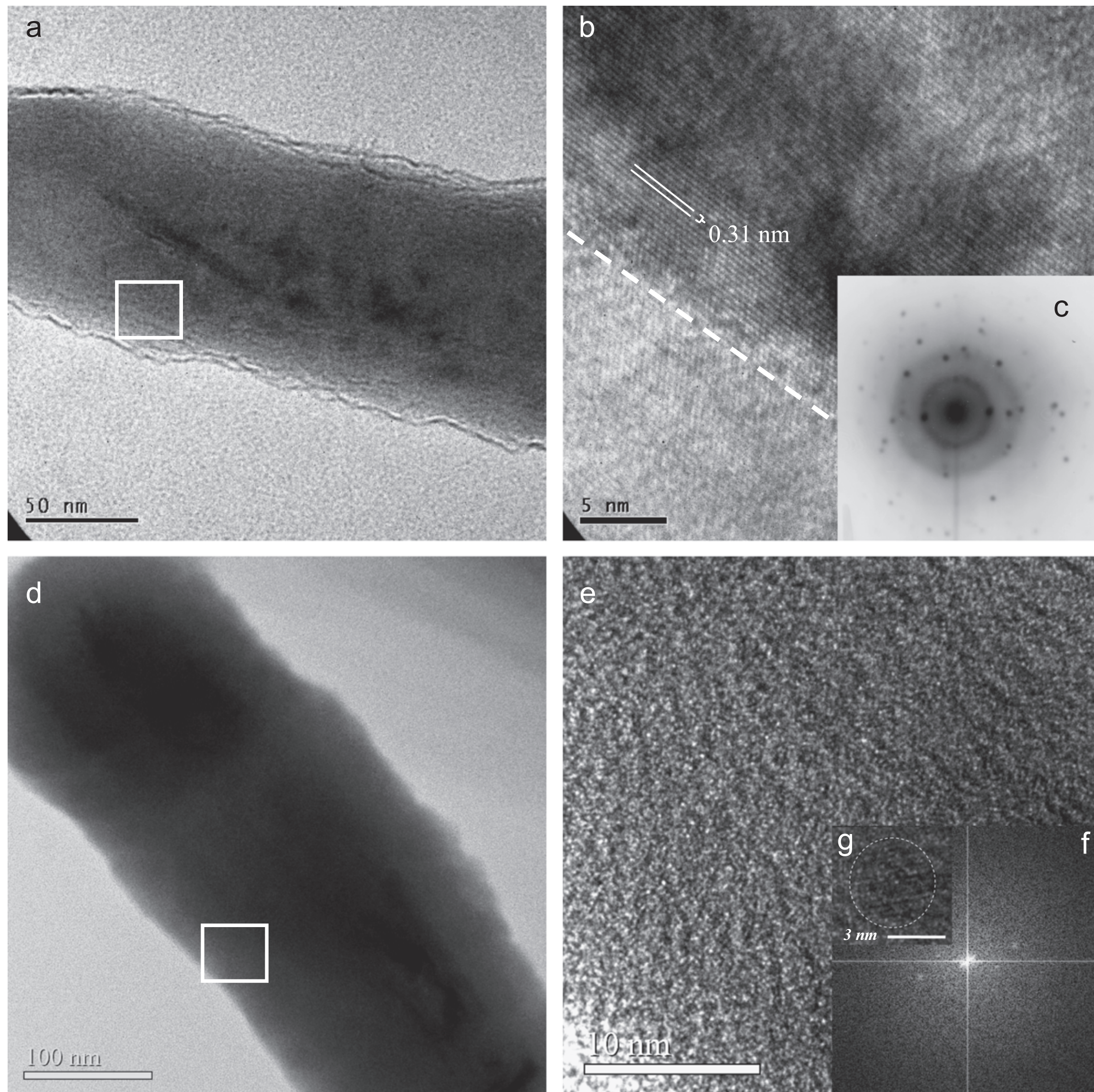

Fig. 4. (a, d) TEM images, (b, e) HRTEM images and (c, f) SAED patterns of the SiNWs synthesize at rf power of 40 and 80 W, respectively. (g) HRTEM image of nanocrystallite Si embedded in SiNWs prepared at rf power of 80 W.

The HRTEM image reveals a large amount of Si nanocrystallites embedded within the amorphous matrix in the NWs. Moreover, the NWs are surrounded by an uncatalyzed amorphous Si layer. This confirms that side wall deposition occurred at rf power of 80 W, which caused the increase in diameter of NWs. Obviously, an increase in rf power to 80 W causes a great decrease in crystallinity and leads to the formation of Si nanocrystallites in SiNWs. This result agrees with the previous reported work [7]. SAED pattern depicted in Fig. 4(f) shows weak spotty crystalline diffractions and an amorphous background, which confirms the existence of nanocrystallites in the SiNWs. The enlarged image of the Si nanocrystallites is depicted in Fig. 4(g). The sizes of the Si nanocrystallites varies from 1 to 4 nm with an average size of 2.8 ± 0.7 nm, which is quite close to the calculation from the Raman spectra. Similar to the SiNWs prepared at 40 W, the nanocrystallites are preferentially oriented in the (111) crystal orientation plane.

Fig. 5(a) and (b) show the typical EDX and Auger electron spectra of the as-prepared SiNWs. The EDX spectrum collected with the electron beam focused on single NWs shows a high amount of Si and a small amount of O and Sn contents. The weak trace of the Sn signal might be due to the diffusion of Sn from the ITO-layer into the SiNWs during the growth process. The C and Cu signals come from the copper supporting grid with a thin layer of carbon covering the mesh. The Si LVV, C, Sn, O and Si KLL Auger peaks correspond to 89, 263, 427, 503 and 1557 to 1614 eV, respectively, as observed from the Auger spectra. Sharp peaks of Si and O indicate high Si and O contents of the as-grown SiNWs, which is contrary to the EDX analysis. The mismatch on O content between the Auger and EDX measurements could be explained by the difference in the two analytic techniques. The penetration of the Auger electron measurement is <5 nm [53], most of the signals are actually obtained from the topmost layer of the NWs. However, EDX with a high penetration power can detect the characteristic X-rays emitted from micrometers of the NWs sample. This is the reason for the appearance of a C signal from the thin layer of carbon in the supporting grid that can be detected from EDX spectroscopy. The high O signal detected by Auger, which appears as only a small amount in the EDX spectra, indicates that the O content resulted from the outer shell of the oxide layer rather than the inner stem of the SiNW. Hence, the O content is ascribed to the surface oxidation of SiNWs after being

Fig. 5. (a) EDX spectrum, (b) Auger electron spectrum and (c) the plot of oxygen (O) to silicon (Si) ratio from EDX and Auger measurement with rf power.

exposed to air. The chemical composition (in %) of Si and O elements are obtained using the existing models on the quantitative analysis of EDX [54] and Auger spectroscopy [55]. The O to Si weight ratio (O W%:Si W%) from EDX and the O to Si concentration ratio (O%:Si%) from the Auger spectra for both SiNWs prepared at 40 and 80 W are plotted in Fig. 5(c). Both measurements show that the SiNWs synthesized at 40 W exhibits higher O to Si ratios compared to the SiNWs prepared at 80 W. The x values of outermost SiO_x layer can be deduced from O%:Si% of the Auger measurement as 0.80 and 0.78 for SiNWs prepared at 40 and 80 W, respectively.

A FTIR measurement was carried out to confirm the surface of Si–O bonding of the SiNWs. We applied an angular reflection technique to obtain the FTIR spectra from SiNWs prepared on ITO coated glass substrate. The angular reflection of the FTIR spectra of SiNWs prepared at rf power of 40 and 80 W are depicted in Fig. 6. The Si–O related absorption bands include 3 TO bands: O–Si–O rocking, $Si–O_x$ bending and Si–O–Si stretching modes corresponding to $\sim$460–520 cm^{-1}, 790–810 cm^{-1} and 1000–1200 cm^{-1}, respectively [56–58], which are observed for the SiNWs prepared at 40 W. Moreover, a weak absorption band located at $\sim$700 cm^{-1} corresponds to $O–Si–H_2$ rotation [59] indicating that there is a H configuration in addition to O in the Si chain of SiNWs. The major absorption bands contributed by the vibration modes of Si–O bonds, which confirm the oxygen passivation on the surface dangling bonds of SiNWs to form thin SiO_x layer. For SiNWs prepared at 80 W, only O–Si–O rocking and Si–O–Si stretching modes are observed in the FTIR spectrum.

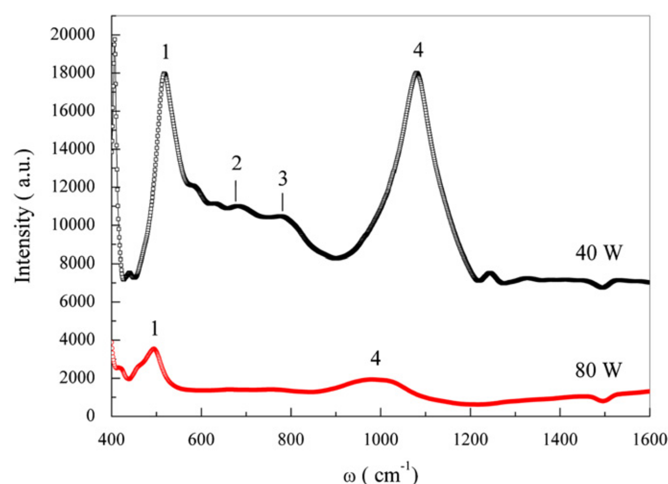

Fig. 6. Angular reflection FTIR spectra of SiNWs prepared at rf power of 40 and 80 W. The absorption band 1, 2, 3 and 4 are attributed to the O–Si–O rocking, $O–Si–H_2$ rotation, $Si–O_x$ bending and Si–O–Si stretching modes, respectively.

The intensities of these two bonds are apparently lower than in SiNWs prepared at 40 W. This again confirms the higher Si–O configuration bonds for SiNWs synthesized at 40 W compared to 80 W.

Fig. 7(a) and (b) show the optical transmission, $T(\lambda)$ and reflectance, $R(\lambda)$ spectra of SiNWs prepared at rf powers of 40 and 80 W. Generally, both SiNWs reveal low T and R in the lower wavelength region. For SiNWs prepared at 40 W, the T decreases from 48.7% at λ=2200 nm to 0% at the absorption edge of $\lambda\sim$500 nm. Meanwhile, the R decreases from 8.8% at λ=2200 nm to $\sim$1% in the visible region. The SiNWs prepared at 80 W shows a considerable reduction in T and R compared to 40 W. Less than 5% of light is transmitted through the SiNWs sample throughout the spectrum with an absorption edge of nearly 1200 nm. The R decreases from 3.3% at λ=2200 nm to $\sim$0.3% in the visible region. Two factors are responsible for the reduction of T and R for SiNWs prepared at 80 W, which are the higher density of SiNWs and the amorphous Si layer covering the sidewalls of the NWs [7]. High densities of SiNWs could increase the possibilities of the internal light interactions within the surface of NW arrays and result in the increase of total internal reflection and optical re-absorption within NWs. Similarly, the amorphous Si layer has effectively suppressed the R due to the enhancement of absorption. The low T and R properties indicate a strong light absorption for the SiNWs. The absorbance (A) and absorption coefficient (α) of the SiNWs can be calculated from the T and R using a relation as [60,61]:

$$A = 100 - T - R \tag{5}$$

$$\alpha = \frac{1}{d}\ln\left(\frac{100-R}{T}\right) \tag{6}$$

where the d is the film thickness in unit of centimeter.

The calculated $A(\lambda)$ and $\alpha(E)$ spectra of SiNWs prepared at 40 and 80 W are plotted in Fig. 7(c) and (d), respectively. The $A(\lambda)$ spectrum of SiNWs prepared at 40 W shows a maximum A of $\sim$99% at 220–500 nm, and decreases abruptly from 500 nm to the longer wavelength. SiNWs prepared at 80 W show a high A of $>$99% over the wavelength range from 220 to $\sim$1500 nm, then slowly decrease to $\sim$86% at 2200 nm. The A of our randomly grown SiNWs is comparable to the optical absorption of samples with a vertically aligned 10 μm long SiNWs ($A>$98% from 300 to 600 nm) reported by Tsakalakos et al. [8] and 1–2 μm of SiNWs arrays (specular reflectance of $<$0.05% in 400–1800 nm) reported by Bae et al. [9]. Meanwhile, Pignalosa et al. [62] recently reported a broad band and wide angle antireflection properties from the randomly oriented crystalline core and amorphous oxide shell SiNWs. This is in agreement with our results showing a high A over a broad wavelength, which could be attributed by strong light trapping ability of the uncatalyzed amorphous layer and nanocrystalline structure of the SiNWs. Generally, the $\alpha(E)$ spectra can be divided into two regions; a high energy region ($E>$1.8 eV), where SiNWs prepared at 40 W reveal higher α compared to 80 W, and vice versa for lower energy region ($E\leq$1.8 eV). This indicates that the SiNWs prepared at 40 W show stronger light trapping properties at the high energy region due to their smaller diameter and highly crystalline structure. The interface states

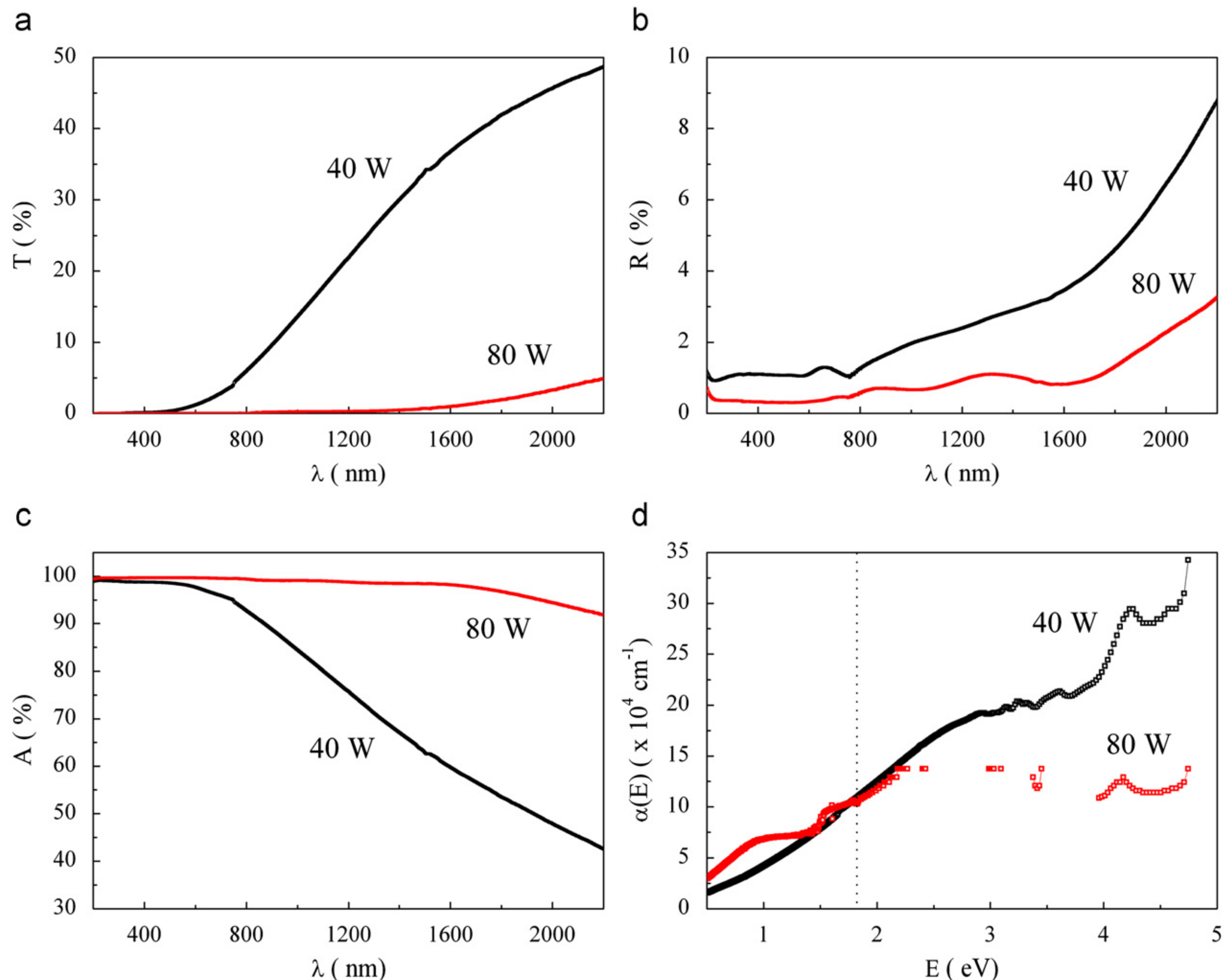

Fig. 7. (a) Optical transmission, $T(\lambda)$, (b) reflectance, $R(\lambda)$, (c) absorbance, $A(\lambda)$ and (d) absorption coefficient, $\alpha(E)$ spectra of SiNWs prepared at rf power of 40 and 80 W.

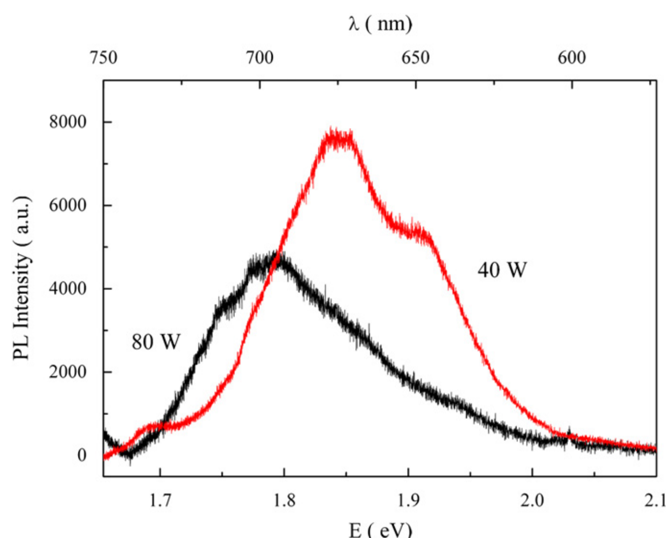

Fig. 8. PL spectra of SiNWs prepared at rf power of 40 and 80 W.

between crystalline SiNWs and SiO_x layer could also play a role in absorbing photons at this region [63]. While, an α broadening at $E \leq 1.8$ eV for SiNWs prepared at 80 W is related to the amorphous band tail, which improve the absorption ability of SiNWs at a lower energy region. Furthermore, both SiNWs exhibited much improvement in α especially at the infrared region (<1.7 eV) compared to bulk Si films.

The PL spectra of SiNWs prepared at rf power of 40 and 80 W are shown in Fig. 8. A broad PL spectrum ranging from 1.73 to 2.05 eV (605–717 nm), which consists of double strong emission bands centered at about 1.84 and 1.92 eV corresponding to the visible red–orange region of 673 and 645 nm, respectively, as revealed for SiNWs synthesized at 40 W. The origin of this emission is attributed to the oxygen related defects states such as peroxy linkage, non bridging oxygen hole centers and oxygen deficient centers [25,26]. Moreover, a weak emission at lower energy of 1.65–1.73 eV (717–752 nm) and centered at $\sim$1.68 eV corresponding to near IR region of 738 nm is observed in the PL spectrum. The rough SiNW sidewall (shown by TEM image) could include nanocrystals of Si, which are surrounded by the outer oxide layer of the SiNWs [24,64]. Meanwhile, the Raman measurement mentioned above also indicates the existence of Si nanocrystallites with size $\sim$4.2 nm within the NWs. Therefore, the longer wavelength PL at $\sim$1.68 eV might be due to the radiative recombination of carriers in Si nanocrystallites formed at the SiO_x/Si interface [24]. Increase in rf power to 80 W results in a blue-shifted and narrower PL broadening range from 1.65 to 1.95 eV (636–752 nm) and centered at $\sim$1.80 eV corresponding to the near IR band of 690 nm. The structural characteristics of the SiNWs prepared at 80 W are expected to directly influence their PL properties. As mentioned above, the crystallite size and crystallinity of SiNWs are much reduced due to the increase of rf power to 80 W. This creates a high density of Si nanocrystallites embedded within the SiNWs. The FTIR spectrum suggests that its Si–O bonds are much weaker than in the SiNWs prepared at 40 W. Hence, the Si nanocrystallites embedded in a-Si matrix and formed at the SiO_x/Si interface mainly contribute to the PL [24,28,65]. The radiative recombination of carriers can produce red emission due to the quantum confinement effect [27]. The origin of the PL are confirmed by applying the relation of PL peak energy, E_{PL} as [64,66]:

$$E_{PL} = E_0 + \frac{3.73}{d^{1.39}} \quad (7)$$

where E_0 is the room temperature band gap of bulk Si of 1.12 eV and d is the crystal size of Si. The calculated crystal sizes, d for the Si nanocrystallites contributed PL peaks for SiNWs prepared at 40 W (1.68 eV) and 80 W (1.80 eV) are 3.9 and 3.4 nm. These values are quite close to the D_R calculated from the Raman peaks, which are 4.2 ± 0.1 and 2.9 ± 0.1 nm for SiNWs prepared at 40 and 80 W, respectively. On the other hand, the PL intensity from our SiNWs is relatively higher compared to several reported works on the light emission of randomly grown SiNWs [25,67]. It is however comparable to the PL intensity produced by oxide-assisted growth of Si/SiO_2 core–shell NWs [68] and chain-like SiNWs [27], but lower than the PL intensity of porous and mesoporous SiNWs [65,69].

4. Conclusions

The structural and optical properties of the SiNWs prepared by hot-wire assisted PECVD technique are highly influenced by the applied rf power. The SiNWs prepared at rf power of 40 W exhibit higly crystalline structure with X_C up to 82.3%, surrounded by a thin layer of SiO_x. Raman and PL analysis suggest the formation of $\sim$4 nm Si nanocrystallites at the Si/SiO_x interface. Meanwhile, SiNWs prepared at rf power of 80 W show significant lower X_C (65.8%) due to the decreases in crystallite size to <4 nm. The NWs are covered by layers of amorphous Si and SiO_x. The high yields of SiNWs at 80 W and the amorphous layer covering the NWs have improved the light absorption over a wide range of wavelengths. The defect states of the surface oxide layer and formation of Si nanocrystallites are the main contributors to the PL at red–orange and near IR regions.

Acknowledgment

This work was supported by the Ministry of Higher Education under a Fundamental Research Grant Scheme (FRGS) of FP002/2010B, by a University Malaya Research Grant (UMRG) of RG061/09AFR and University of Malaya Postgraduate Research Fund (PPP) of PV019/2011B. The authors would also like to acknowledge Interscience Sdn. Bhd. and Renishaw (UK) for the Raman and PL measurements.

References

[1] J.-J. Niu, J.-N. Wang, Mater. Lett. 62 (2008) 767.
[2] Z.Q. Liu, S.S. Xie, W.Y. Zhou, L.F. Sun, Y.B. Li, D.S. Tang, X.P. Zou, C.Y. Wang, G. Wang, J. Cryst. Growth 224 (2001) 230.
[3] Th. Stelzner, G. Andra, E. Wendler, W. Wesch, R. Scholz, U. Gosele, S. Christiansen, Nanotechnology 17 (2006) 2895.
[4] Y. Cui, L.J. Lauhon, M.S. Gudiksen, J. Wang, C.M. Lieber, Appl. Phys. Lett. 78 (2001) 2214.
[5] S. Hofmann, C. Ducati, R.J. Neill, S. Piscanec, A.C. Ferrari, J. Geng, R. Dunin-Borowsky, J. Robertson, J. Appl. Phys. 94 (2003) 6005.
[6] L. Yu, B.O. Donnell, P.-J. Alet, S. Conesa-Boj, F. Peiro, J. Arbiol, P.R.i. Cabarrocas, Nanotechnology 20 (2009) 225604.
[7] M.M. Adachi, M.P. Anantram, K.S. Karim, Nano Lett. 10 (2010) 4903.
[8] L. Tsakalakos, J. Balch, J. Fronheiser, M.-Y. Shih, S.F. LeBoeuf, M. Pietrykowski, P.J. Codella, B.A. Korevaar, O. Sulima, J. Rand, A. Davuluru, U. Rapol, J. Nanophotonics 1 (2007) 013552.
[9] J. Bae, H. Kim, X.-M. Zhang, C.H. Dang, Y. Zhang, Y.J. Choi, A. Nurmikko, Z.L. Wang, Nanotechnology 21 (2010) 095502.
[10] L. Hu, G. Chen, Nano Lett. 7 (2007) 3249.
[11] J. Zhu, Z. Yu, G.F. Burkhard, C.-M. Hsu, S.T. Connor, Y. Xu, Q. Wang, M. McGehee, S. Fan, Y. Cui, Nano Lett. 9 (2009) 279.
[12] E. Garnett, P. Yang, Nano lett. 10 (2010) 1082.
[13] M.D. Kelzenberg, S.W. Boettcher, J.A. Petykiewicz, D.B. Turner-Evans, M.C. Putnam, E.L. Warren, J.M. Spurgeon, R.M. Briggs, N.S. Lewis, H.A. Atwater, Nat. Mater. 9 (2010) 239.
[14] Z.G. Bai, D.P. Yu, J.J. Wang, Y.H. Zou, W. Qian, J.S. Fu, S.Q. Feng, J. Xu, L.P. You, Mater. Sci. Eng. B 72 (2000) 117.

[15] D.P. Yu, Z.G. Bai, J.J. Wang, Y.H. Zou, W. Qian, J.S. Fu, H.Z. Zhang, Y. Ding, G.C. Xiong, L.P. You, J. Xu, S.Q. Feng, Phys. Rev. B 59 (1999) R2498.
[16] J.D. Holmes, K.P. Johnston, R.C. Doty, B.A. Korgel, Science 287 (2000) 1471.
[17] X.C. Wu, W.H. Song, K.Y. Wang, T. Hu, B. Zhao, Y.P. Sun, J.J. Du, Chem. Phys. Lett. 336 (2000) 53.
[18] Y.-C. Peng, Z.-D. Fan, Z.-H. Bai, X.-W. Zhao, J.-Z. Lou, X. Cheng, Chin. Phys. Lett. 27 (2010) 057305.
[19] B. Gelloz, Y. Coffinier, B. Salhi, N. Koshida, G. Patriarche, R. Boukherroub, Mater. Res. Soc. Proc. 958 (2007) 179.
[20] B. Salhi, B. Gelloz, N. Koshida, G. Patriarche, R. Boukherroub, Phys. Status Solidi (a) 204 (2007) 1302.
[21] S.T. Lee, N. Wang, C.S. Lee, Mater. Sci. Eng. A 286 (2000) 16.
[22] X.T. Zhou, R.Q. Zhang, H.Y. Peng, N.G. Shang, N. Wang, I. Bello, C.S. Lee, S.T. Lee, Chem. Phys. Lett. 332 (2000) 215.
[23] T.V. Torchynska, M.M. Rodriguez, F.G.B. Espinoza, L.Y. Khomenkova, N.E. Korsunska, L.V. Scherbina, Phys. Rev. B 65 (2001) 115313.
[24] S.M. King, S. Chaure, S. Krishnamurthy, W.J. Blau, A. Colli, A.C. Ferrari, J. Nanosci. Nanotechnol. 8 (2008) 4202.
[25] X.B. Zeng, X.B. Liao, B. Wang, S.T. Dai, Y.Y. Xu, X.B. Xiang, Z.H. Hu, H.W. Diao, G.L. Kong, J. Cryst. Growth 265 (2004) 94.
[26] T.K. Sham, S.J. Naftel, P.S.G. Kim, R. Sammynaiken, Y.H. Tang, I. Coulthard, A. Moewes, J.W. Freeland, Y.F. Hu, S.T. Lee, Phys. Rev. B 70 (2004) 045313.
[27] X.H. Sun, N.B. Wong, C.P. Li, S.T. Lee, T.K. Sham, J. Appl. Phys. 96 (2004) 3447.
[28] D.D.D. Ma, S.T. Lee, J. Shinar, Appl. Phys. Lett. 87 (2005) 033107.
[29] M.L.A. Rigout, H. Niu, C. Qin, L. Zhang, C. Li, X. Bai, N. Fan, Nanotechnology 19 (2008) 245303.
[30] W. Chern, K. Hsu, I.S. Chun, B.P. de Azeredo, N. Ahmed, K.-H. Kim, J.-M. Zuo, N. Fang, P. Ferreira, X. Li, Nano Lett. 10 (2010) 1582.
[31] F. Demami, L. Pichon, R. Rogel, A.C. Salaun, IOP Conf. Ser.: Mater. Sci. Eng. 6 (2009) 012014.
[32] X. Sun, R. Tao, L. Lin, Z. Li, Z. Zhang, J. Feng, Appl. Surf. Sci. 257 (9) (2011) 3861.
[33] T.-C. Wong, C.-C. Yu, J.-J. Wu, Adv. Funct. Mater. 15 (2005) 1440.
[34] S. Bhattacharya, D. Banerjee, K.W. Adu, S. Samui, S. Bhattacharyya, Appl. Phys. Lett. 85 (2004) 2008.
[35] H.F. Yan, Y.J. Xing, Q.L. Hang, D.P. Yu, Y.P. Wang, J. Xu, Z.H. Xi, S.Q. Feng, Chem. Phys. Lett. 323 (2000) 224.
[36] Y.Y. Wong, M. Yahaya, M.M. Salleh, B.Y. Majlis, Sci. Technol. Adv. Mater. 6 (2005) 330.
[37] Z.Q. Liu, Z.W. Pan, L.F. Sun, D.S. Tang, W.Y. Zhou, G. Wong, L.X. Qian, S.S. Xie, J. Phys. Chem. Solids 61 (2000) 1171.
[38] X.D. Bai, Z. Xu, S. Liu, E.G. Wang, Sci. Technol. Adv. Mater. 6 (2005) 804.
[39] R. Rurali, Rev. Mod. Phys. 82 (2010) 427.
[40] J.T. Yin, M. Wada, K. Yamamoto, Y. Kitano, S. Tanase, T. Sakai, J. Electrochem. Soc. 153 (2006) A472.
[41] Y.-G. Jung, S.-W. Jee, J.-H. Lee, J. Appl. Phys. 102 (2007) 046102.
[42] P.-J. Alet, L. Yu, G. Patriarche, S. Palacin, P.R.i. Cabarrocas, J. Mater. Chem. 18 (2008) 5187.
[43] S.K. Chong, B.T. Goh, Z. Aspanut, M.R. Muhamad, C.F. Dee, S.A. Rahman, Thin Solid Films 519 (2011) 4933.
[44] M. Mattila, T. Hakkarainen, H. Lipsanen, H. Jiang, E.I. Kauppinen, Appl. Phys. Lett. 89 (2006) 063119.
[45] B. Li, D. Yu, S. Zhang, Phys. Rev. B 59 (1999) 1645.
[46] C.Y. Meng, J.L. Chen, S.C. Lee, in: Proceedings of the 5th IEEE Conference on Nanotechnology, Nagoya, Japan, July 2005.
[47] S. Piscanec, A.C. Ferrari, M. Cantoro, S. Hofmann, J.A. Zapien, Y. Lifshitz, S.T. Lee, J. Robertson, Mater. Sci. Eng. C 23 (2003) 931.
[48] H. Scheel, S. Reich, A.C. Ferrari, M. Cantoro, A. Colli, C. Thomsen, Appl. Phys. Lett. 88 (2006) 233114.
[49] S.K. Chong, B.T. Goh, Z. Aspanut, M.R. Muhamad, C.F. Dee, S.A. Rahman, Appl. Surf. Sci. 257 (2011) 3320.
[50] D. Han, K. Wang, Sol. Energy Mater. Sol. Cells 78 (2003) 181.
[51] S. Mukhopadhyay, C. Das, S. Ray,, J. Phys. D: Appl. Phys. 37 (2004) 1736.
[52] A. Gajovic, D. Gracin, K. Juraic, J. Sancho-Parramon, M. Ceh, Thin Solid Films 517 (2009) 5453.
[53] G. Ecke, V. Cimalla, K. Tonisch, V. Lebedev, H. Romanus, O. Ambacher, J. Liday, J. Electr. Eng. 58 (2007) 301.
[54] P.J. Goodhew, J. Humphreys, R. Beanland, Electron Microscopy and Analysis, Taylor & Francis, New York, 2001. (pp. 175–181).
[55] K. Tsutsumi, Y. Nagasawa, JEOL News 38 (2003) 41.
[56] S. Wan, Y. Yu, J. Zhang, J. Non-Cryst. Solids 355 (2009) 518.
[57] J. Niu, D. Yang, J. Sha, J.N. Wang, M. Li, Mater. Lett. 61 (2007) 894.
[58] Q. Hu, H. Suzuki, H. Gao, H. Araki, W. Yang, T. Noda, Chem. Phys. Lett. 378 (2003) 299.
[59] B.S. Swain, B.P. Swain, N.M. Hwang, Curr. Appl. Phys. 10 (2010) S439.
[60] C. Lin, M.L. Povinelli, Opt. Express 17 (2009) 19371.
[61] W.Q. Hong, J. Phys. D: Appl. Phys. 22 (1989) 1384.
[62] AIP Advances, vol. 1, 2011, p. 032124.
[63] B.S. Swain, B.P. Swain, N.M. Hwang, Mater. Chem. Phys. 129 (2011) 733.
[64] A.I. Hochbaum, D. Gargas, Y.J. Hwang, P. Yang, Nano Lett. 9 (2009) 3550.
[65] V.A. Sivakov, F. Voigt, A. Berger, G. Bauer, S.H. Christiansen, Phys. Rev. B 82 (2010) 125446.
[66] G. Ledoux, O. Guillois, D. Porterat, C. Reynaud, F. Huisken, B. Kohn, V. Paillard, Phys. Rev. B 62 (2000) 15942.
[67] F. Shi, J. Lin, Y. Huang, J. Zhang, C. Tang, Mater. Chem. Phys. 118 (2009) 125.
[68] A. Colli, S. Hofmann, A. Fasoli, A.C. Ferrari, C. Ducati, R.E. Dunin-Borkowski, J. Robertson, Appl. Phys. A 85 (2006) 247.
[69] L. Lin, S. Guo, X. Sun, J. Feng, Y. Wang, Nanoscale Res. Lett. 5 (2010) 1822.